

## Enhancing organic–inorganic hybrid solar cell efficiency using rod–coil diblock polymer additive

Cite this: *J. Mater. Chem. A*, 2013, **1**, 665

Jhih-Fong Lin,<sup>a</sup> Wei-Che Yen,<sup>b</sup> Chun-Yu Chang,<sup>a</sup> Yang-Fang Chen<sup>\*c</sup>  
and Wei-Fang Su<sup>\*ab</sup>

Organic–inorganic hybrid bulk heterojunction (BHJ) solar cells have attracted much attention due to their low cost fabrication, flexibility, and long life. However, the compatibility between organic and inorganic materials is still an issue that needs to be solved to achieve high power conversion efficiency (PCE). The larger size and dense characteristics of inorganic nanocrystals make it hard to control the morphology and phase separation of organic–inorganic hybrid thin films by conventional processes like thermal annealing and solvent annealing. In this study, we have carried out a systematic investigation using an additive: rod–coil diblock copolymer poly(3-hexyl thiophene)-*b*-poly(2-vinyl pyridine) (P3HT-*b*-P2VP) to P3HT:TiO<sub>2</sub> to make a ternary system. That improves the compatibility between the P3HT homopolymer and the TiO<sub>2</sub> nanorod hybrid materials and results in enhanced performance of the hybrid solar cell. The hydrophobic characteristics of the P3HT segment of the copolymer are compatible with the P3HT homopolymer, and the P2VP segment, containing a pyridine moiety is more compatible with hydrophilic TiO<sub>2</sub>. The results of atomic force microscopy and X-ray diffraction spectroscopy studies of hybrid films reveal that the crystallization behavior of the homopolymer P3HT in the film can be tuned by incorporating different weight ratios of P3HT-*b*-P2VP. The efficiency of charge separation is also improved as observed by greater photoluminescence quenching. Furthermore, the power conversion efficiency of the solar cell fabricated from this new hybrid system was increased threefold as compared with the one without the additive (1.20% vs. 0.42%), which indicates that the amphiphilic P3HT-*b*-P2VP can effectively modulate the interfacial interactions between the conducting polymer and nanocrystals in both solution and film to have the appropriate morphology for high efficient solar cells.

Received 31st August 2012  
Accepted 15th October 2012

DOI: 10.1039/c2ta00142j

[www.rsc.org/MaterialsA](http://www.rsc.org/MaterialsA)

### Introduction

Recently, organic bulk-heterojunction (BHJ) solar cells have drawn much attention for renewable energy due to such advantages as its low cost, light weight, flexibility, and ease of large-scale fabrication. Traditionally, the BHJ solar cell is fabricated from materials consisting of a donor and acceptor. The donor is a conducting polymer which absorbs sunlight and generates excitons.<sup>1–4</sup> The acceptor can be fullerene derivatives<sup>5–7</sup> or inorganic nanocrystals which mostly transport electrons.<sup>8–11</sup> The power conversion of BHJ solar cells consists of several steps. Firstly, the conducting polymer absorbs light and generates excitons which must diffuse to the interfaces of donor–acceptor and dissociate into charge carriers of electrons and holes. Then, charge carriers are transported through

corresponding percolation paths to the opposite electrode to generate electricity. The degree of charge separation depends on the extent of phase separation, including size and amount. The diffusion length of excitons is rather small at less than 10 nm. Once the size of phase separation exceeds the diffusion length, the excitons will not be separated but lost as heat, which is one of the main reasons for poor device performance. In addition, appropriate phase separation can help the thin film of BHJs to form a continuous pathway for efficient charge transport. Therefore, a way to control the morphology properly in BHJs to have adequate interfaces and paths for efficient charge separation and transport needs to be addressed and investigated.

Among various acceptor materials, fullerene derivatives such as [6,6]-phenyl-C61-butyric acid methyl ester (PC<sub>61</sub>BM) is commonly used in organic BHJ solar cells due to its good compatibility with conducting polymers. By thermal annealing<sup>12–15</sup> or solvent annealing,<sup>16–18</sup> the morphology and phase separation of this BHJ thin film can be optimized for best device performance. However, the extended thermal treatment would induce severe phase separation, which degrades the device performance. This kind of poor thermal stability is the main

<sup>a</sup>Department of Materials Science and Engineering, National Taiwan University, Taipei 10617, Taiwan. E-mail: wfsu@ntu.edu.tw; Fax: +886-2-3366-4078; Tel: +886-2-3366-4078

<sup>b</sup>Institute of Polymer Science and Engineering, National Taiwan University, Taipei 10617, Taiwan

<sup>c</sup>Department of Materials Science and Engineering, National Taiwan University, Taipei 10617, Taiwan. E-mail: yfchen@ntu.edu.tw; Tel: +886-2-3366-5125

reason why the polymer/fullerene solar cell has difficulty becoming a viable commercial product.

On the other hand, inorganic nanocrystals with good thermal and solvent stability have become potential candidates for acceptors to replace fullerene derivatives in organic BHJ solar cells. By adjusting the conditions of synthesis, the size, composition, and band structure of inorganic nanocrystals, one can easily tune the nanocrystals to meet the desired chemical and physical properties for solar cells. However, the incompatibility between conducting polymers and nanocrystals is still an obstacle to achieve high power conversion efficiencies. Meanwhile, the large size and dense features of nanocrystals also make the film morphology difficult to control by common treatments such as thermal and/or solvent annealing.

To have better control of morphology in polymer–nanocrystal BHJs, we have investigated different *in situ* solution deposition processes for highly ordered nanostructures.<sup>19,20</sup> By adding fluoro additives into the blend of P3HT homopolymers and TiO<sub>2</sub> nanorods, we have promoted vertical phase separation to improve charge transport. Although many studies have demonstrated approaches to reduce the degree of phase separation between conducting polymers and nanocrystals, they are not yet well developed for highly efficient solar cells.<sup>21,22</sup>

In recent years, self-assembled block copolymers have been developed to form highly ordered nanostructures using simple solution processes.<sup>23–27</sup> Various nanostructures can be obtained, depending on the type and composition of each segment of copolymer. Additionally, with specific functional groups placed on the main chain or side chain of the segment of copolymers, they can be like a mold to confine certain kind of nanocrystals. Furthermore, rod–coil diblock copolymers were applied in organic photovoltaic devices for forming long-range continuous transport paths and improving the device performance.<sup>28–31</sup> The rod segment is made of conducting polymers, such as polythiophene and the coil segment is usually a relatively flexible insulating polymer, such as poly(vinyl pyridine) or poly(methyl methacrylate). This block copolymer has improved the thermal stability of polymer–fullerene solar cells through the stabilization of phase separated fullerene without aggregation in BHJ, but it does not confine fullerene in its specific segment or domain of the copolymer. Thus, the copolymer does not enhance the performance of polymer–fullerene solar cells. On the other hand, if the copolymer can confine the inorganic nanocrystals within its ordered structure and avoid the formation of large size aggregates in polymer–nanocrystal hybrid films, one can expect, the rod–coil diblock copolymer will improve the performance of polymer–nanocrystal solar cells.

In our previous studies,<sup>32</sup> we have demonstrated that a solar cell fabricated from a P3HT:TiO<sub>2</sub> nanorod BHJ has better thermal stability than that of P3HT–fullerene BHJs. However, the compatibility between P3HT and TiO<sub>2</sub> nanorods needs to be improved for better power conversion efficiency. We have successfully synthesized self assembled P3HT-*b*-P2VP diblock copolymers *via* anionic macroinitiation.<sup>33</sup> The copolymer was mixed with nicotinic acid-modified TiO<sub>2</sub> nanoparticles to fabricate a solar cell. The TiO<sub>2</sub> nanoparticles were preferentially confined in the P2VP domain and instead of randomly forming

micro-sized phase segregation, an ordered nanostructure and excellent photoluminescence (PL) quenching were observed in the film P3HT-*b*-P2VP:TiO<sub>2</sub>.<sup>34</sup> As a result, the device fabricated from P3HT-*b*-P2VP:TiO<sub>2</sub> hybrid material exhibited more than a 30-fold improvement in power conversion efficiency as compared to that of 0.3 P3HT–0.7 P2VP blend:TiO<sub>2</sub>. However, the power conversion efficiency of the P3HT-*b*-P2VP:TiO<sub>2</sub> hybrid solar cell is still too low to have actual usage. The main problem is the insulating P2VP segment which hinders the charge transport from the P3HT segment and lowers the output photocurrent. In this study, we used a small amount of P3HT-*b*-P2VP as an additive to improve the compatibility between P3HT and TiO<sub>2</sub>, and to enhance the formation of nanostructures in the P3HT:TiO<sub>2</sub> hybrid film. A close to threefold increase in device performance has been achieved. The correlation between morphology change and device performance with different amounts of P3HT-*b*-P2VP were systematically studied and established.

## Experimental section

All the chemicals were used as received without further purification. The anatase TiO<sub>2</sub> nanorods were synthesized by hydrolysis of titanium tetraisopropoxide (TTIP) according to our previously work.<sup>35</sup> Oleic acid (OA, 120 g) was vigorously stirred at 120 °C for one hour in a three-neck flask under argon flow to remove moisture. The solution was then cooled to 98 °C and titanium tetraisopropoxide (17 mmol, Aldrich, 99.999%), as the precursor, was added into the flask and stirred for 5 min to mix well with the oleic acid. Trimethylamine-*N*-oxide dihydrate (34 mmol, Acros, 98%) in 17 mL of water was rapidly injected into the flask as the catalyst of the hydrolysis reaction. This reaction was continued for 9 h to complete the hydrolysis and crystallization, and the TiO<sub>2</sub> nanorods were obtained. The TiO<sub>2</sub> nanorods were purified through several cycles of washing and precipitation using methanol to remove any unreacted oleic acid and impurities.

The as-synthesized TiO<sub>2</sub> was capped with insulating OA ligand. To remove the OA ligand on the TiO<sub>2</sub> surface, the ligand was exchanged by pyridine. First, the TiO<sub>2</sub>–OA nanorods (20 mL) were washed and precipitated by methanol (20 mL) four times to remove OA molecules that were not tightly bound to the surface. Then, pyridine (20 mL) was added to the washed TiO<sub>2</sub> nanorods by an ultrasonic homogenizer. The mixture was then placed into a three-neck flask and refluxed at 70 °C for 24 h under nitrogen to obtain a transparent solution. We called the product TiO<sub>2</sub>–pyridine. The P3HT-*b*-P2VP was synthesized according to our previous work.<sup>33</sup> Furthermore, the conducting P3HT homopolymer was synthesized by the Industrial Technology Research Institute of Taiwan; the molecular weight of P3HT is 65 kDa; polydispersity (PDI) and regioregularity (RR) are 1.39 ± 0.06 and >95%, respectively.

The fabrication process of hybrid thin films with the ternary P3HT:P3HT-*b*-P2VP:TiO<sub>2</sub> system is in accordance with the following procedure. First, the PEDOT:PSS solution (Baytron P VP AI 4083) was filtrated through a 0.20 μm PVDF filter and spin-coated on cleaned ITO glass (Luminescence Technology

Corp., 10  $\Omega$ ) as a hole transport layer. The PEDOT:PSS/ITO substrates were put in an oven and dried at 120  $^{\circ}\text{C}$  for 40 minutes to remove the moisture. For preparing the ternary P3HT:P3HT-*b*-P2VP:TiO<sub>2</sub> solution, we first dissolved P3HT homopolymer in chlorobenzene with a concentration of 30 mg mL<sup>-1</sup>, then the TiO<sub>2</sub> nanorods were redispersed in solvent mixture (pyridine : dichloromethane : chloroform = 1 : 2 : 3) with a concentration of 12.5 mg mL<sup>-1</sup>. Then, P3HT-*b*-P2VP diblock copolymers were dissolved into chloroform and mixed with TiO<sub>2</sub> solution first. In this step, the TiO<sub>2</sub> nanorods were supposed to be dispersed well in the P2VP domain. Then, the P3HT-*b*-P2VP:TiO<sub>2</sub> solution was added into the P3HT solution and kept stirring at 50  $^{\circ}\text{C}$  overnight. We found the hybrid solution with P3HT-*b*-P2VP is much clearer after cooling to room temperature than the neat P3HT:TiO<sub>2</sub> solution. This shows that P3HT-*b*-P2VP plays a role as surfactant between P3HT and TiO<sub>2</sub>, and it also avoids the aggregation of TiO<sub>2</sub> in solution state. Then, the hybrid solution was spin-coated onto the PEDOT:PSS thin film and the thickness is about 120 nm. To reduce charge recombination at the interface between the active layer and cathode, a 20 nm TiO<sub>2</sub> nanorod layer was directly spin coated on the active layer as a hole blocking layer. Then the sample was stored in a glove box for 1 day to remove the residual solvent. After finishing the above steps, a 100 nm aluminum layer was thermally evaporated as the cathode.

Atomic force microscopy (Digital Instruments, Nanoscopes III) was employed to observe the morphology changes of the P3HT:P3HT-*b*-P2VP:TiO<sub>2</sub> ternary hybrid thin film. We also used wide-angle X-ray diffraction spectroscopy (BL 13A1, National Synchrotron Radiation Research Center, Taiwan) to study the crystallization behavior of the P3HT homopolymer. A solar simulator (Newport, Model 66902) and voltage source meter (Keithley, Model 2410) were used for OPV device measurements.

## Results and discussion

In P3HT:TiO<sub>2</sub> hybrid thin film, the poor compatibility between the P3HT homopolymer and inorganic nanocrystals of TiO<sub>2</sub> induces severe aggregation, *i.e.* a large degree of phase separation (Fig. 1(a)). Thus, the interactions between P3HT and TiO<sub>2</sub> are decreased, which results in low efficiency of charge separation. This may be the main reason for the low power conversion efficiency in P3HT:TiO<sub>2</sub> hybrid solar cells. The chemical structure of the rod-coil diblock copolymer P3HT-*b*-P2VP and a schematic diagram of the interaction between the P2VP segment and TiO<sub>2</sub> are shown in Fig. 1(b). In P3HT-*b*-P2VP, the P2VP segment is more compatible with TiO<sub>2</sub> than the P3HT segment owing to the presence of polar pyridine in the P2VP segment. By adding a small amount of P3HT-*b*-P2VP into the P3HT:TiO<sub>2</sub> hybrid thin film, the extent of P3HT homopolymer aggregation can be reduced.

In polymer-inorganic BHJ solar cells, the poor compatibility between conducting polymers and inorganic nanocrystals has been observed in many studies.<sup>36–38</sup> The blending of two materials tends to directly induce phase separation. To observe the extent of phase separation between the P3HT homopolymer and TiO<sub>2</sub> nanorods, we prepared P3HT:TiO<sub>2</sub> hybrid films with

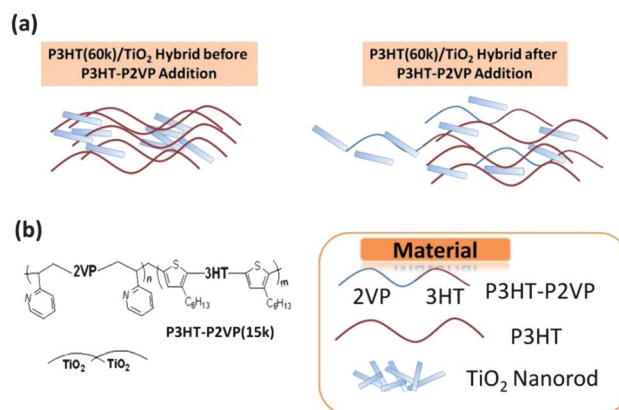


**Fig. 1** (a) Schematic diagram of P3HT-TiO<sub>2</sub> hybrid thin film with and without P3HT-*b*-P2VP. (b) Chemical structure of rod-coil diblock copolymer P3HT-*b*-P2VP and a schematic diagram of P2VP-TiO<sub>2</sub> interactions.

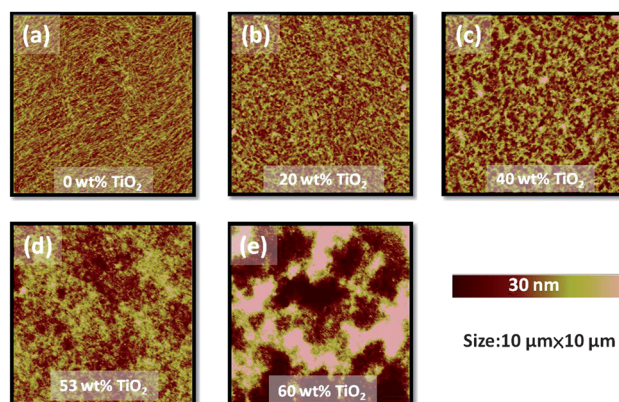


**Fig. 2** Morphology of different P3HT:TiO<sub>2</sub> hybrid films with (a) 0 wt%, (b) 20 wt%, (c) 40 wt%, (d) 53 wt%, and (e) 60 wt% of TiO<sub>2</sub>. The size of the AFM phase image is 10  $\mu\text{m}$   $\times$  10  $\mu\text{m}$ .

different weight ratios of the two components. Fig. 2 shows the aggregation of each phase is growing with increasing amount of TiO<sub>2</sub> in the blend. The neat P3HT film exhibits nanowire features with a length exceeding 3  $\mu\text{m}$  (Fig. 2(a)). The formation of such P3HT nanowires may be attributed to a mixture of chlorobenzene, dichloromethane, chloroform, and pyridine with different boiling temperatures and varying solubility for P3HT. During the spin coating process, the different evaporation rates of each solvent would induce the crystallization of P3HT. Meanwhile, the addition of TiO<sub>2</sub> makes the morphology of the hybrid film become rougher; P3HT and TiO<sub>2</sub> are aggregated into microdomains, respectively, which confirms the poor compatibility between P3HT and TiO<sub>2</sub> (Fig. 2(b)–(e)). Thus, by increasing TiO<sub>2</sub> loading, it did not increase the interactions between the two components, but promotes the formation of aggregates with reduced interfaces. That results in low efficiency charge separation and low power conversion efficiency.

To reduce the formation of aggregates in P3HT:TiO<sub>2</sub> hybrid thin films, we incorporated a small amount of the rod-coil diblock copolymer P3HT-*b*-P2VP into the hybrid to confine the TiO<sub>2</sub> nanorods in the P2VP domain rather than forming

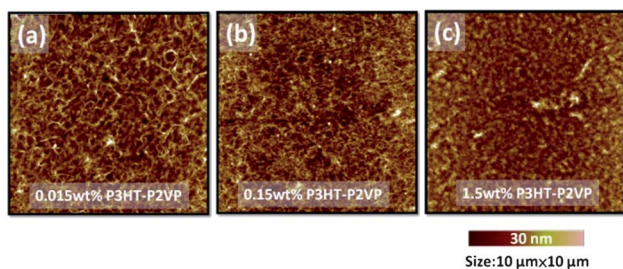


**Fig. 3** Morphology of different P3HT films with (a) 0.015 wt%, (b) 0.15 wt%, (c) 1.5 wt% P3HT-*b*-P2VP. The size of the AFM phase image is 10 μm × 10 μm.

aggregates. The amount of P3HT-*b*-P2VP is limited at low concentration at less than or equal to 1.5 wt% to avoid any insulating effect on establishing continuous percolation paths for P3HT and TiO<sub>2</sub>, respectively. The P3HT-*b*-P2VP can not only reduce the aggregation of TiO<sub>2</sub>, but can also improve the solubility of P3HT in poor solvents such as pyridine and dichloromethane. The P2VP segment can be easily dissolved into the above solvents, and the P3HT segment can lower the interfacial tension and improve the stability of the P3HT homopolymer in this solvent mixture without gelling. To clarify the influence of P3HT-*b*-P2VP in the P3HT:TiO<sub>2</sub> hybrid system, we first investigated the effect of P3HT-*b*-P2VP on neat P3HT homopolymer. Fig. 3 shows the topography of the P3HT thin film with different amounts of P3HT-*b*-P2VP. At 0.015 wt%, the P3HT-*b*-P2VP made the morphology of P3HT homopolymer become entangled wires (Fig. 3(a)). Comparing the morphology of the neat P3HT homopolymer thin film (Fig. 2(a)), such entangled nanowires indicate that the interfacial tension is lowered after the addition

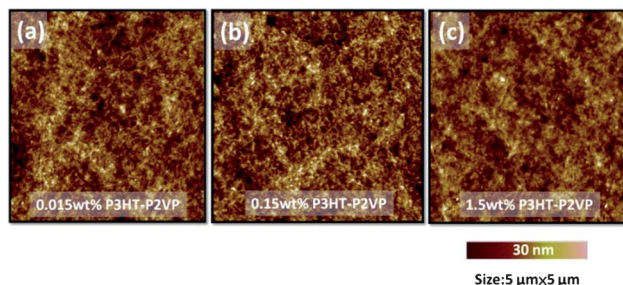


**Fig. 4** Morphology of different P3HT:TiO<sub>2</sub> hybrid films with (a) 0.015 wt%, (b) 0.15 wt%, (c) 1.5 wt% P3HT-*b*-P2VP. The size of the AFM phase image is 5 μm × 5 μm.

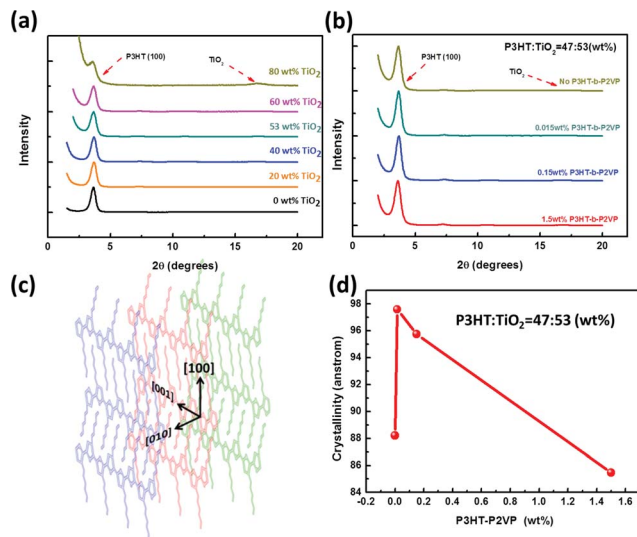


**Fig. 5** X-Ray diffraction patterns of hybrid films (a) at different blending ratios of P3HT:TiO<sub>2</sub> and (b) with different added amounts of P3HT-*b*-P2VP at blending ratio of 47 : 53. (c) Schematic diagram of P3HT homopolymer crystallite and corresponding direction and (d) crystal size of P3HT homopolymer in (100) direction with incorporation of different wt% of P3HT-*b*-P2VP.

of P3HT-*b*-P2VP, and the straight and long P3HT homopolymer chains are difficult to form during evaporation of the solvent. With increasing amount of P3HT-*b*-P2VP, the feature of P3HT nanowires gradually disappears, and finally transforms to clusters (Fig. 3(c)). In this study, such long P3HT nanowires (>3 μm) are believed to be not suitable for efficient organic-inorganic photovoltaics. Although the high crystallinity of P3HT nanowires could facilitate charge transport in one direction, fewer interfaces with TiO<sub>2</sub> result in reduced charge separation and low device performance. In Fig. 2(d), it clearly indicates the formation of TiO<sub>2</sub> and P3HT nanowire aggregates in the P3HT:TiO<sub>2</sub> hybrid thin film with a weight ratio of 47 : 53. After the incorporation of P3HT-*b*-P2VP, the length of the P3HT nanowires is shorter and the feature of the P3HT homopolymer could also be transformed from nanowires to clusters (Fig. 4). Considering the diffusion length of excitons (10 nm), we speculate that the P3HT clusters have more interfaces to interact with TiO<sub>2</sub> for efficient charge separation. To evaluate the changes in P3HT crystallization after the incorporation of P3HT-*b*-P2VP, X-ray diffraction spectroscopy was used to determine the size of P3HT crystallinity that can qualify the extent of phase separation in the

**Table 1** Summary of crystallization behaviors of P3HT homopolymer with the addition of P3HT-*b*-P2VP by wide-angle X-ray diffraction spectroscopy

wt% of P3HT homopolymer	wt% of P3HT- <i>b</i> -P2VP	P3HT (100) peak (degree)	FWHM (degree)	Crystal size (nm)
100	0	1.82	0.46	11.50
80	0	1.84	0.52	10.23
60	0	1.84	0.52	10.12
47	0	1.82	0.60	8.82
40	0	1.83	0.60	8.87
47	0.015	1.83	0.54	9.76
47	0.15	1.84	0.55	9.58
47	1.5	1.81	0.62	8.55

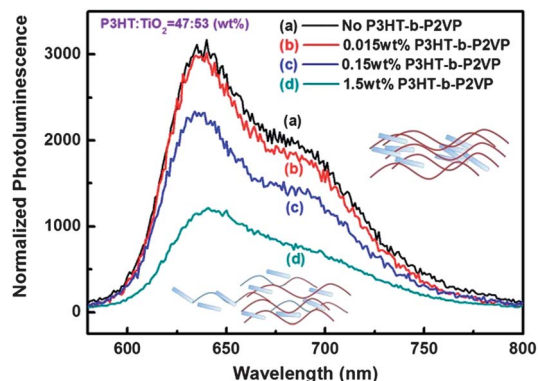


**Fig. 6** Photoluminescence spectra of different P3HT:TiO<sub>2</sub> hybrid films with and without P3HT-*b*-P2VP additive.

P3HT:TiO<sub>2</sub> hybrid. The results of X-ray diffraction were summarized in Table 1. We found that the crystallite size in the P3HT homopolymer (100) plane decreases from 11.50 nm to 8.87 nm as the content of TiO<sub>2</sub> increased to 60 wt%. However, according to the corresponding AFM images, the P3HT homopolymer nanowires are still clearly observed (Fig. 2(e)).

The decrease of crystallite size may come from the disruption of the TiO<sub>2</sub> nanorods. Furthermore, the crystallization behavior of the P3HT homopolymer was also affected by incorporation of P3HT-*b*-P2VP into the P3HT:TiO<sub>2</sub> hybrid with a weight ratio of 47 : 53. At 0.015 wt% or 0.15 wt%, the crystallite size of the P3HT homopolymer could be increased from 8.82 nm to 9.76 nm or to 9.58 nm, respectively, but its size decreases at 1.5 wt% (8.82 nm to 8.55 nm), as indicated in Table 1 and Fig. 5(d). Two mechanisms are competing with each other that influence the crystallization behavior of the P3HT homopolymer while adding the copolymer into the hybrid. Initially, a small amount of P3HT-*b*-P2VP helps to dissolve the P3HT homopolymer well in poor solvents (pyridine, dichloromethane, and chloroform), so the homopolymer chain can extend well in this solvent mixture and induce large-scale crystallization during the spin-coating process. Then, at higher concentrations of copolymer, the reduction of crystallite size of the P3HT homopolymer indicates that TiO<sub>2</sub> nanorods were well dispersed in the P3HT

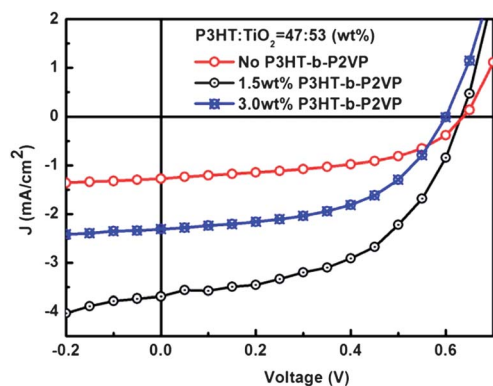


**Fig. 7** Photovoltaic device performance of different P3HT:TiO<sub>2</sub> hybrid films with and without P3HT-*b*-P2VP.

**Table 2** Photovoltaic performance of P3HT:TiO<sub>2</sub> hybrid system containing different amounts of P3HT-*b*-P2VP additive

Sample	$V_{OC}$ (volts)	$J_{SC}$ (mA cm <sup>-2</sup> )	Fill factor (%)	PCE (%)
No P3HT- <i>b</i> -P2VP	0.64	1.27	50.45	0.41
1.5 wt% P3HT- <i>b</i> -P2VP	0.64	3.69	51.40	1.20
3.0 wt% P3HT- <i>b</i> -P2VP	0.60	2.31	52.85	0.73

homopolymer. That results in the suppression of P3HT homopolymer crystallization. Furthermore, we found the quenching of photoluminescence of the hybrid film is decreased with increasing amount of P3HT-*b*-P2VP, as shown in Fig. 6. This observation supports our speculation of increased charge separation due to improved compatibility and increased interface interaction between the P3HT homopolymer and TiO<sub>2</sub> nanorods. We believe that the effect of the P3HT-*b*-P2VP additive for P3HT and TiO<sub>2</sub> nanorods in the hybrid solution and the spin-coating process, respectively, is the following. The incorporation of P3HT-*b*-P2VP functions as a surfactant and enhances the solubility of P3HT in the solvent mixture. Thus, the entropy of P3HT is increased with the presence of copolymer in the hybrid solution. During the spin-coating process, the reduced entropy nanowire of P3HT in the hybrid film is difficult to form with the evaporation of the mixed solvents. Furthermore, the P3HT-*b*-P2VP is also a surfactant for TiO<sub>2</sub> nanorods to be more compatible with the P3HT homopolymer which makes TiO<sub>2</sub> nanorods disperse well with P3HT to obtain a good smooth film. As a result, we can conclude that the P3HT-*b*-P2VP functions as an effective surfactant to modulate the crystallization of P3HT in the hybrid film formation process.

Finally, we fabricated the P3HT:TiO<sub>2</sub> hybrid thin film containing P3HT-*b*-P2VP into solar cells and their performances are shown in Fig. 7 and summarized in Table 2. After incorporating 1.5 wt% P3HT-*b*-P2VP into the active layer, the main enhancement of device performance is from short circuit current density (from 1.27 mA cm<sup>-2</sup> to 3.69 mA cm<sup>-2</sup>). This 2.9 fold improvement of the short-circuit current density is expected from the increased interface interactions and improved charge separation, as discussed above. Furthermore, the P3HT-*b*-P2VP also prevents the severely aggregated phase separation between the P3HT homopolymer and TiO<sub>2</sub> nanorods which increases the extent of continuous network formation. As a result, the fill factor also increases from 50.45% to 51.40%, and the power conversion efficiency was improved from 0.41% to 1.20%. However, the device performance decreases to 0.73% after the amount of P3HT-*b*-P2VP reaches 3 wt%. The lower open-circuit voltage and short-circuit current indicate the excess insulating P2VP segment hinders the charge transfer and increases the charge recombination.

## Conclusion

In summary, we have demonstrated that the rod-coil diblock copolymer P3HT-*b*-P2VP can effectively modulate the morphology and phase separation of P3HT:TiO<sub>2</sub> hybrid films

for enhanced performance of solar cells. The copolymer functions as an interlayer between the P3HT homopolymer and TiO<sub>2</sub>. The P3HT segment of the copolymer improves the solubility of the P3HT homopolymer, and the P2VP segment makes the TiO<sub>2</sub> nanorods compatible with the P3HT homopolymer, as indicated in the topographic and XRD studies of the hybrid films. The film becomes smoother with less aggregation by increasing the concentration of copolymer. The crystallite size of the P3HT homopolymer in the presence of copolymer increased initially at a low concentration of 0.015 wt% due to the improved solubility for both polymer and TiO<sub>2</sub>. The crystallite size decreases at a relatively high concentration of 1.5 wt% due to the disruption of TiO<sub>2</sub>, but that increases the interface interactions and charge separation of the hybrid. Thus, the device fabricated from the P3HT:TiO<sub>2</sub> hybrid thin film containing 1.5 wt% P3HT-*b*-P2VP has close to 3 times higher power conversion efficiency than the device fabricated from the hybrid thin film without additive (0.42% vs. 1.20%).

## Acknowledgements

Financial support obtained from the National Science Council of Taiwan (NSC 101-3113-E-002-010, and NSC 101-2120-M-002-003) is highly appreciated.

## References

- 1 N. Blouin, A. Michaud and M. Leclerc, *Adv. Mater.*, 2007, **19**, 2295–2300.
- 2 Y. Y. Liang, Y. Wu, D. Q. Feng, S. T. Tsai, H. J. Son, G. Li and L. P. Yu, *J. Am. Chem. Soc.*, 2009, **131**, 56–57.
- 3 L. J. Huo, J. H. Hou, H. Y. Chen, S. Q. Zhang, Y. Jiang, T. L. Chen and Y. Yang, *Macromolecules*, 2009, **42**, 6564–6571.
- 4 H. Y. Chen, J. H. Hou, S. Q. Zhang, Y. Y. Liang, G. W. Yang, Y. Yang, L. P. Yu, Y. Wu and G. Li, *Nat. Photonics*, 2009, **3**, 649–653.
- 5 Y. J. Cheng, C. H. Hsieh, Y. J. He, C. S. Hsu and Y. F. Li, *J. Am. Chem. Soc.*, 2010, **132**, 17381–17383.
- 6 P. P. Khlyabich, B. Burkhardt and B. C. Thompson, *J. Am. Chem. Soc.*, 2011, **133**, 14534–14537.
- 7 J. G. Labram, J. Kirkpatrick, D. D. C. Bradley and T. D. Anthopoulos, *Adv. Energy Mater.*, 2011, **1**, 1176–1183.
- 8 Y. F. Zhou, M. Eck and M. Kruger, *Energy Environ. Sci.*, 2010, **3**, 1851–1864.
- 9 S. Q. Ren, L. Y. Chang, S. K. Lim, J. Zhao, M. Smith, N. Zhao, V. Bulovic, M. Bawendi and S. Gradecak, *Nano Lett.*, 2011, **11**, 3998–4002.
- 10 K. M. Noone, E. Strein, N. C. Anderson, P. T. Wu, S. A. Jenekhe and D. S. Ginger, *Nano Lett.*, 2010, **10**, 2635–2639.
- 11 H. C. Chen, C. W. Lai, I. C. Wu, H. R. Pan, I. W. P. Chen, Y. K. Peng, C. L. Liu, C. H. Chen and P. T. Chou, *Adv. Mater.*, 2011, **23**, 5451–5455.
- 12 M. Campoy-Quiles, T. Ferenczi, T. Agostinelli, P. G. Etchegoin, Y. Kim, T. D. Anthopoulos, P. N. Stavrinou, D. D. C. Bradley and J. Nelson, *Nat. Mater.*, 2008, **7**, 158–164.
- 13 L. G. Li, G. H. Lu, S. J. Li, H. W. Tang and X. N. Yang, *J. Phys. Chem. B*, 2008, **112**, 15651–15658.
- 14 X. N. Yang, J. Loos, S. C. Veenstra, W. J. H. Verhees, M. M. Wienk, J. M. Kroon, M. A. J. Michels and R. A. J. Janssen, *Nano Lett.*, 2005, **5**, 579–583.
- 15 D. Chen, F. Liu, C. Wang, A. Nakahara and T. P. Russell, *Nano Lett.*, 2011, **11**, 2071–2078.
- 16 S. S. van Bavel, E. Sourty, G. de With and J. Loos, *Nano Lett.*, 2009, **9**, 507–513.
- 17 A. J. Parnell, A. D. F. Dunbar, A. J. Pearson, P. A. Staniec, A. J. C. Dennison, H. Hamamatsu, M. W. A. Skoda, D. G. Lidzey and R. A. L. Jones, *Adv. Mater.*, 2010, **22**, 2444–2447.
- 18 G. J. Zhao, Y. J. He and Y. F. Li, *Adv. Mater.*, 2010, **22**, 4355–4358.
- 19 Y. C. Huang, G. C. Welch, G. C. Bazan, M. L. Chabinyc and W. F. Su, *Chem. Commun.*, 2012, **48**, 7250–7252.
- 20 H. C. Liao, C. H. Lee, Y. C. Ho, M. H. Jao, C. M. Tsai, C. M. Chuang, J. J. Shyue, Y. F. Chen and W. F. Su, *J. Mater. Chem.*, 2012, **22**, 10589–10596.
- 21 L. Zhao, X. C. Pang, R. Adhikary, J. W. Petrich, M. Jeffries-EL and Z. Q. Lin, *Adv. Mater.*, 2011, **23**, 2844–2849.
- 22 M. He, F. Qiu and Z. Q. Lin, *J. Mater. Chem.*, 2011, **21**, 17039–17048.
- 23 S. A. Jenekhe and X. L. Chen, *Science*, 1998, **279**, 1903–1907.
- 24 S. A. Jenekhe and X. L. Chen, *Science*, 1999, **283**, 372–375.
- 25 B. de Boer, U. Stalmach, H. Nijland and G. Hadziioannou, *Adv. Mater.*, 2000, **12**, 1581–1583.
- 26 H. A. Klok and S. Lecommandoux, *Adv. Mater.*, 2001, **13**, 1217–1229.
- 27 V. Ho, B. W. Boudouris, B. L. McCulloch, C. G. Shuttle, M. Burkhardt, M. L. Chabinyc and R. A. Segalman, *J. Am. Chem. Soc.*, 2011, **133**, 9270–9273.
- 28 N. G. Kang, B. Cho, B. G. Kang, S. Song, T. Lee and J. S. Lee, *Adv. Mater.*, 2012, **24**, 385–390.
- 29 J. H. Tsai, Y. C. Lai, T. Higashihara, C. J. Lin, M. Ueda and W. C. Chen, *Macromolecules*, 2010, **43**, 6085–6091.
- 30 C. Yang, J. K. Lee, A. J. Heeger and F. Wudl, *J. Mater. Chem.*, 2009, **19**, 5416–5423.
- 31 C. C. Chueh, T. Higashihara, J. H. Tsai, M. Ueda and W. C. Chen, *Org. Electron.*, 2009, **10**, 1541–1548.
- 32 Y. C. Huang, J. H. Hsu, Y. C. Liao, W. C. Yen, S. S. Li, S. T. Lin, C. W. Chen and W. F. Su, *J. Mater. Chem.*, 2011, **21**, 4450–4456.
- 33 C. A. Dai, W. C. Yen, Y. H. Lee, C. C. Ho and W. F. Su, *J. Am. Chem. Soc.*, 2007, **129**, 11036–11038.
- 34 W. C. Yen, Y. H. Lee, J. F. Lin, C. A. Dai, U. S. Jeng and W. F. Su, *Langmuir*, 2011, **27**, 109–115.
- 35 T. W. Zeng, Y. Y. Lin, H. H. Lo, C. W. Chen, C. H. Chen, S. C. Liou, H. Y. Huang and W. F. Su, *Nanotechnology*, 2006, **17**, 5387–5392.
- 36 H. Borchert, *Energy Environ. Sci.*, 2010, **3**, 1682–1694.
- 37 I. Lokteva, N. Radychev, F. Witt, H. Borchert, J. Parisi and J. Kolny-Olesiak, *J. Phys. Chem. C*, 2010, **114**, 12784–12791.
- 38 Y. C. Huang, J. H. Hsu, Y. C. Liao, W. C. Yen, S. S. Li, S. T. Lin, C. W. Chen and W. F. Su, *J. Mater. Chem.*, 2011, **21**, 4450–4456.